

Study on the effects of 5d energy locations of Ce³⁺ ions on NIR quantum cutting process in Y₂SiO₅: Ce³⁺, Yb³⁺

Wenli Zhou,¹ Jie Yang,¹ Jing Wang,^{1,*} Ye Li,¹ Xiaojun Kuang,¹ Jinke Tang,²
and Hongbin Liang¹

¹Ministry of Education Key Laboratory of Bioinorganic and Synthetic Chemistry, State Key Laboratory of Optoelectronic Materials and Technologies, KLGHEI of Environment and Energy Chemistry, School of Chemistry and Chemical Engineering, Sun Yat-sen University, Guangzhou, 510275, China

²Department of Physics and Astronomy, University of Wyoming, Laramie, WY 82071, USA
ceswj@mail.sysu.edu.cn

Abstract: The effects of the 5d energy locations of Ce³⁺ centers on the NIR quantum cutting process were studied in Y₂SiO₅ with two different substitutional Y³⁺ lattice sites for Ce³⁺ and Yb³⁺. Powder XRD and Rietveld refinement were used to characterize phase purity, crystal structure, lattice parameters and occupation fractions of Y_{2-x-y}Ce_xYb_ySiO₅ ($x = 0.002$ and 0.3 , $y = 0-0.2$). PLE and PL spectra show that both kinds of Ce³⁺ centers in Y_{2-x-y}Ce_xYb_ySiO₅ can cooperatively transfer energy to Yb³⁺-Yb³⁺ ions pair. The dependence of the integrated emission intensities of Ce³⁺ and Yb³⁺, decay lifetime (τ) of Ce³⁺, nonradiative energy transfer rate ($K_{Ce \rightarrow Yb}$), cooperative energy transfer efficiency (η_{CET}) and quantum efficiency (η_{QE}) on the concentration of Yb³⁺ ions were studied in details. More importantly, these results demonstrate that the 5d energy locations of Ce³⁺ ions have a great influence on NIR quantum cutting process in Ce³⁺-Yb³⁺ system: the closer they are to twice the absorption energy (~ 20000 cm⁻¹) of Yb³⁺, the higher the cooperative energy transfer efficiency from the lowest 5d excited state of Ce³⁺ to the Yb³⁺-Yb³⁺ ions pair.

©2012 Optical Society of America

OCIS codes: (160.5690) Rare-earth-doped materials; (300.6280) Spectroscopy, fluorescence and luminescence; (260.2160) Energy transfer.

References and links

1. Q. Y. Zhang and X. Y. Huang, "Recent progress in quantum cutting phosphors," *Prog. Mater. Sci.* **55**(5), 353–427 (2010).
2. B. M. van der Ende, L. Aarts, and A. Meijerink, "Near-Infrared Quantum Cutting for Photovoltaics," *Adv. Mater. (Deerfield Beach Fla.)* **21**(30), 3073–3077 (2009).
3. B. M. van der Ende, L. Aarts, and A. Meijerink, "Lanthanide ions as spectral converters for solar cells," *Phys. Chem. Chem. Phys.* **11**(47), 11081–11095 (2009).
4. W. Shockley and H. J. Queisser, "Detailed Balance Limit of Efficiency of p-n Junction Solar Cells," *J. Appl. Phys.* **32**(3), 510–519 (1961).
5. T. Trupke, M. A. Green, and P. Würfel, "Improving solar cell efficiencies by down-conversion of high-energy photons," *J. Appl. Phys.* **92**(3), 1668–1674 (2002).
6. J. M. Meijer, L. Aarts, B. M. van der Ende, T. J. H. Vlugt, and A. Meijerink, "Downconversion for solar cells in YF₃:Nd³⁺, Yb³⁺," *Phys. Rev. B* **81**(3), 035107–035116 (2010).
7. X. Y. Huang, D. C. Yu, and Q. Y. Zhang, "Enhanced near-infrared quantum cutting in GdBO₃:Tb³⁺, Yb³⁺ phosphors by Ce³⁺ codoping," *J. Appl. Phys.* **106**(11), 113521 (2009).
8. L. Aarts, B. M. van der Ende, M. F. Reid, and A. Meijerink, "Downconversion for Solar Cells in YF₃:Pr³⁺, Yb³⁺," *Spectrosc. Lett.* **43**(5), 373–381 (2010).
9. J. T. van Wijngaarden, S. Scheidelaar, T. J. H. Vlugt, M. F. Reid, and A. Meijerink, "Energy transfer mechanism for downconversion in the (Pr³⁺, Yb³⁺) couple," *Phys. Rev. B* **81**(15), 155112 (2010).
10. P. Vergeer, T. J. H. Vlugt, M. H. F. Kox, M. I. den Hertog, J. P. J. M. van der Eerden, and A. Meijerink, "Quantum cutting by cooperative energy transfer in Yb_xY_{1-x}PO₄: Tb³⁺," *Phys. Rev. B* **71**(1), 014119–014129 (2005).
11. J. D. Chen, H. Guo, Z. Q. Li, H. Zhang, and Y. X. Zhuang, "Near-infrared quantum cutting in Ce³⁺, Yb³⁺ co-doped YBO₃ phosphors by cooperative energy transfer," *Opt. Mater.* **32**(9), 998–1001 (2010).

12. X. F. Liu, Y. Teng, Y. X. Zhuang, J. H. Xie, Y. B. Qiao, G. P. Dong, D. P. Chen, and J. R. Qiu, "Broadband conversion of visible light to near-infrared emission by Ce³⁺, Yb³⁺-codoped yttrium aluminum garnet," *Opt. Lett.* **34**(22), 3565–3567 (2009).
13. J. Ueda and S. Tanabe, "Visible to near infrared conversion in Ce³⁺-Yb³⁺ Co-doped YAG ceramics," *J. Appl. Phys.* **106**(4), 043101–043105 (2009).
14. J. J. Zhou, Y. Teng, G. Lin, X. Q. Xu, Z. J. Ma, and J. R. Qiu, "Broad-Band Excited Quantum Cutting in Eu²⁺-Yb³⁺ Co-doped Aluminosilicate Glasses," *J. Electrochem. Soc.* **157**(8), B1146–B1148 (2010).
15. Q. H. Zhang, J. Wang, G. G. Zhang, and Q. Su, "UV photon harvesting and enhanced near-infrared emission in novel quantum cutting Ca₂BO₃Cl:Ce³⁺, Tb³⁺, Yb³⁺ phosphor," *J. Mater. Chem.* **19**(38), 7088–7092 (2009).
16. G. G. Zhang, C. M. Liu, J. Wang, X. J. Kuang, and Q. Su, "A dual-mode solar spectral converter CaLaGa₃S₆O:Ce³⁺, Pr³⁺: UV-Vis-NIR luminescence properties and solar spectral converting mechanism," *J. Mater. Chem.* **22**(5), 2226–2232 (2012).
17. D. Q. Chen, Y. S. Wang, Y. L. Yu, P. Huang, and F. Y. Weng, "Quantum cutting downconversion by cooperative energy transfer from Ce³⁺ to Yb³⁺ in borate glasses," *J. Appl. Phys.* **104**(11), 116105 (2008).
18. A. A. Coelho, TOPAS ACADEMIC. Brisbane, Australia, 2005, version 4.
19. B. A. Maksimov, V. V. Ilyukhin, Y. A. Kharitonov, and N. V. Belov, "Crystal structure of yttrium oxyorthosilicate Y₂O₃SiO₂ and Y₂SiO₅," *Kristallografiya* **15**, 926–933 (1970).
20. R. D. Shannon, "Revised Effective Ionic Radii and Systematic Studies of Interatomic Distances in Halides and Chalcogenides," *Acta Crystallogr. A* **32**(5), 751–767 (1976).
21. L. Pidola, O. Guillot-Noëla, A. Kahn-Hararia, B. Viana, D. Pelenc, and D. Gouriera, "EPR study of Ce³⁺ ions in lutetium silicate scintillators Lu₂Si₂O₇ and Lu₂SiO₅," *J. Phys. Chem. Solids* **67**(4), 643–650 (2006).
22. A. Denoyer, S. Jandl, B. Viana, O. Guillot-Noel, P. Goldner, D. Pelenc, and F. Thibault, "Optical properties of Yb-doped Y₂SiO₅ thin films," *Opt. Mater.* **30**(3), 416–422 (2007).
23. S. Campos, A. Denoyer, S. Jandl, B. Viana, D. Vivien, P. Loiseau, and B. Ferrand, "Spectroscopic studies of Yb³⁺-doped rare earth orthosilicate crystals," *J. Phys.-Condens. Mat.* **16**, 4579–4590 (2004).
24. H. Jiao, F. H. Liao, S. J. Tian, and X. P. Jing, "Influence of rare earth Sc and La to the luminescent properties of FED blue phosphor Y₂SiO₅: Ce," *J. Electrochem. Soc.* **151**(7), J39–J42 (2004).
25. H. Yokota, M. Yoshida, H. Ishibashi, T. Yano, H. Yamamoto, and S. Kikkawa, "Concentration effect of cerium in (Y_{0.9-x}Gd_{0.1}Ce_x)₂SiO₅ blue phosphor," *J. Alloy. Comp.* **495**(1), 162–166 (2010).
26. E. Coetsee, J. J. Terblans, O. M. Ntwaaborwa, and H. C. Swart, "Luminescent mechanism of Y₂SiO₅:Ce phosphor powder," *Physica B* **404**(22), 4426–4430 (2009).
27. H. Feng, V. Jary, E. Mihokova, D. Ding, M. Nikl, G. Ren, H. Li, S. Pan, A. Beitlerova, and R. Kucerkova, "Temperature dependence of luminescence characteristics of Lu_{2(1-x)}Y_{2x}SiO₅: Ce³⁺ scintillator grown by the Czochralski method," *J. Appl. Phys.* **108**(3), 033519–033524 (2010).
28. H. Matsui, C. N. Xu, Y. Liu, and T. Watanabe, "Optical Spectroscopy of Ce³⁺-Activated X₂-Y₂SiO₅," *J. Ceram. Soc. Jpn.* **108**(1263), 1003–1006 (2000).
29. R. B. Jabbarova, C. Chartier, B. G. Tagieva, O. B. Tagiev, N. N. Musayeva, C. Barthou, and P. Benalloul, "Radiative properties of Eu²⁺ in BaGa₂S₄," *J. Phys. Chem. Solids* **66**(6), 1049–1056 (2005).
30. S. Saha, P. S. Chowdhury, and A. Patra, "Luminescence of Ce³⁺ in Y₂SiO₅ nanocrystals: Role of crystal structure and crystal size," *J. Phys. Chem. B* **109**(7), 2699–2702 (2005).
31. B. Han, H. B. Liang, Y. Huang, Y. Tao, and Q. Su, "Vacuum Ultraviolet-Visible Spectroscopic Properties of Tb³⁺ in Li(Y, Gd)(PO₃)₄: Tunable Emission, Quantum Cutting, and Energy Transfer," *J. Phys. Chem. C* **114**(14), 6770–6777 (2010).

1. Introduction

Near-infrared (NIR) quantum cutting (QC) is expected as an important method to modify the solar spectrum [1]. In a typical process, one UV-Vis (300–500 nm) photon is cut into two or more NIR (~1000 nm) photons, which perfectly match the maximum spectral response of a *c*-Si solar cell ($E_g \approx 1.12\text{eV}$, $\lambda \approx 1100\text{ nm}$). It can realize multiple electron-hole pairs generation per incident photon in the *c*-Si solar cell, greatly reducing energy losses due to charge thermalization and improving the solar cell efficiencies [2,3]. Trupke and co-authors theoretically demonstrated that the Shockley-Queisser limiting efficiency of 30% can be substantially increased up to 40% through a down-conversion of high-energy photons [4,5]. This work prompted worldwide research on NIR QC luminescent materials. Up to now, most of the research has focused on Ln³⁺-Yb³⁺ couples [6–15], where Ln³⁺ ions serve as donors that utilize the UV-green fraction of the solar spectrum and Yb³⁺ ions serve as acceptors that give NIR emissions at ~1000 nm. According to the electronic configuration of rare-earth ions, these couples are classified into two groups: Ln³⁺-Yb³⁺ (Ln = Pr, Nd, Tb, Ho, Er, Tm) and Ce³⁺/Eu²⁺-Yb³⁺. The former Ln³⁺ ions have the narrow absorption peaks with low efficiency in the UV-green region [7–10]. The latter Ce³⁺/Eu²⁺ ions show broad absorption bands with high efficiency in the region [12–14, 16]. Therefore, the Ce³⁺/Eu²⁺-Yb³⁺ couple is an ideal NIR QC system as a solar spectral converter for *c*-Si solar cell [3].

NIR QC luminescent materials with the $Ce^{3+}/Eu^{2+}-Yb^{3+}$ couples have been reported in various systems, including chloroborate phosphor, YAG ceramics, and borate and aluminosilicate glasses [13–15,17]. Cooperative energy transfer (CET) mechanism was mostly proposed to explain the quantum cutting UV-to-NIR energy transfer from Ce^{3+}/Eu^{2+} to Yb^{3+} in those systems mentioned above. Figure 1 shows the typical CET processes involving Tb^{3+} and Ce^{3+} ions: Both Tb^{3+} and Ce^{3+} ions directly and respectively absorb a high energy photon via the forbidden $4f-4f$ transition and allowed $4f \rightarrow 5d$ transitions; then transfer the excitation energy to two Yb^{3+} ions under the assistance of phonons; finally two NIR photons are produced. Unlike the constant 5D_4 level ($\sim 20000 \text{ cm}^{-1}$) of Tb^{3+} , the locations of the $5d$ energy levels of Ce^{3+} ions are easily affected by the crystal field. It varies significantly from 27027 cm^{-1} in borate glasses to 26596 cm^{-1} in YBO_3 phosphor and to 20000 cm^{-1} in YAG ceramics [11,13,17]. The energy differences (ΔE) between the lowest $5d$ excited state of Ce^{3+} in these materials and twice the energy ($\sim 20000 \text{ cm}^{-1}$) of the $^2F_{5/2} \rightarrow ^2F_{7/2}$ transition of the Yb^{3+} ions are about 7027 cm^{-1} (ΔE_1), 6596 cm^{-1} (ΔE_2) and 0 cm^{-1} (ΔE_3), respectively. The QC process in $Tb^{3+}-Yb^{3+}$ couples is almost resonant cooperative energy transfer. On the contrary, the process in $Ce^{3+}-Yb^{3+}$ couples strongly depends on the energy locations of the lowest $5d$ excited state of Ce^{3+} ions in specific compounds. Obviously, the composition and crystal structure of host compounds, local symmetry of lattice sites, phonon frequency, etc., play key roles in the CET process involving the $Ce^{3+}-Yb^{3+}$ couples and determine the NIR quantum efficiency. Unfortunately, these issues seem to have been overlooked in previous researches on the cooperative QC process in $Ce^{3+}/Eu^{2+}-Yb^{3+}$ systems.

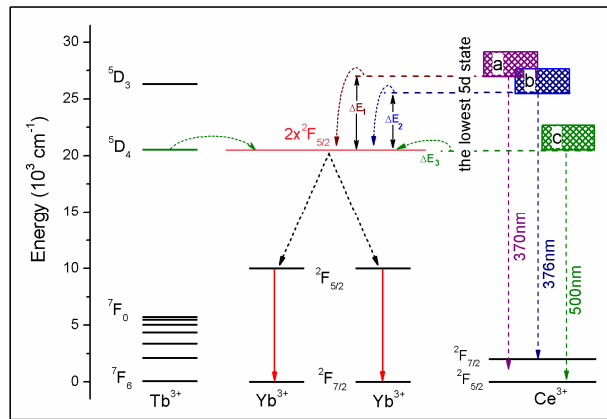


Fig. 1. Schematic energy level diagram on QC process of $Tb^{3+}-Yb^{3+}$ and $Ce^{3+}-Yb^{3+}$ couples in some specific systems: (a) borate glasses; (b) YBO_3 phosphor and (c) YAG ceramics.

In this work, we aim to investigate how and to what extent the energy locations of the lowest $5d$ excited state of Ce^{3+} ions affect the NIR quantum efficiency in $Ce^{3+}-Yb^{3+}$ couples. We limit our investigation to the $X_2-Y_2SiO_5$ system with two different crystallographic sites [$Y^{3+}(1)$ and $Y^{3+}(2)$] that Ce^{3+} and Yb^{3+} substitute to exclude the influence of other factors on the cooperative QC process, such as phonon vibration frequency, nonradiative centers and crystal structure. The influence of these mentioned factors can be considered exactly the same for the two kinds of Ce^{3+} centers in a given host lattice. The dependences of the integrated emission intensities of Ce^{3+} and Yb^{3+} , decay lifetime (τ) of Ce^{3+} , nonradiative energy-transfer rate ($K_{Ce \rightarrow Yb}$), cooperative energy transfer efficiency (η_{CET}) and quantum efficiency (η_{QE}) on the Yb^{3+} concentration (y) were studied in details. More importantly, these results demonstrate that the closer to twice the $^2F_{7/2}-^2F_{5/2}$ absorption energy ($\sim 20000 \text{ cm}^{-1}$) of Yb^{3+} ion is the $5d$ energy location of Ce^{3+} ion, the higher the CET efficiency in $Ce^{3+}-Yb^{3+}$ couple. We believe that this work may be of great significance for designing advanced NIR QC phosphors for Si based solar cell applications.

2. Experimental

A series of silicates compounds were prepared in solid state reactions. Stoichiometric amounts of Y_2O_3 (99.99%), SiO_2 (AR), CeO_2 (99.99%) and Yb_2O_3 (99.99%) were ground and mixed homogeneously in an agate mortar for 30 min. Then the mixtures were placed in alumina crucibles with covers and fired at 1400 °C in a reducing atmosphere (CO) for 12 h. Finally, the samples were cooled to room temperature in the furnace and reground into powders for subsequent analysis.

The phase purity of the product was examined by X-ray diffraction (XRD) using a D8 ADVANCE powder diffractometer with $\text{Cu-K}\alpha$ radiation ($\lambda = 1.54059 \text{ \AA}$) at room temperature. The high quality XRD data for Rietveld refinement was collected over a 2θ range from 10° to 90° at an interval of 0.02° with a counting time of 8 sec per step. Structural refinement of XRD data was performed using the TOPAS-Academic program [18]. The photoluminescence (PL), excitation (PLE) spectra and the decay curves were obtained using a FSP920 Time Resolved and Steady State Fluorescence Spectrometer (Edinburgh Instruments) at room temperature and 10 K, which was equipped with a 450W Xe lamp, a 150w nF900 flash lamp, red sensitive PMT and R5509-72 NIR-PMT in a liquid nitrogen cooled housing (Hamamatsu Photonics K.K.).

3. Results and discussion

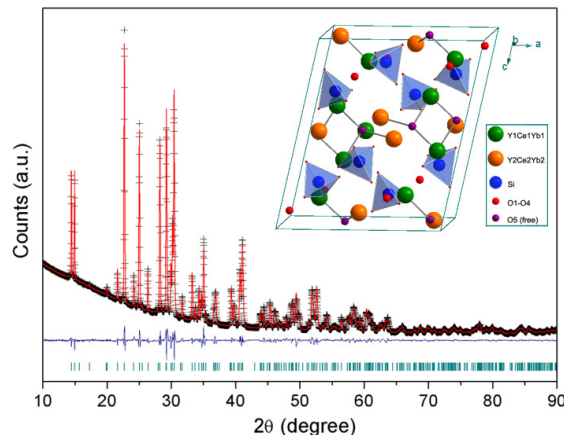


Fig. 2. Experimental (crosses) and calculated (red solid line) XRD patterns and their difference (blue solid line) for $\text{Y}_{1.64}\text{Ce}_{0.3}\text{Yb}_{0.06}\text{SiO}_5$. One set of tick mark shows the Bragg reflection positions of the phase $\text{Y}_{1.64}\text{Ce}_{0.3}\text{Yb}_{0.06}\text{SiO}_5$. Inset: the crystal structure of corresponding unit cell.

The phase purity of all products $\text{Y}_{2-x}\text{Ce}_x\text{Yb}_y\text{SiO}_5$ ($x = 0.002$ and 0.3 ; $y = 0, 0.02, 0.06, 0.1, 0.14, 0.2, 0.3, 0.4$) was examined and their XRD patterns are similar to each other. As a representative, the experimental (crosses) XRD pattern of $\text{Y}_{1.64}\text{Ce}_{0.3}\text{Yb}_{0.06}\text{SiO}_5$ is shown in Fig. 2. The Rietveld refinement was performed on this compound using the $\text{I}12/a1$ structure model reported by Maksimov et al. [19], which converged to $R_{\text{wp}} = 3.66\%$ and $R_{\text{B}} = 1.47\%$. The refined lattice constants and cell volumes are $a = 10.5267(2) \text{ \AA}$, $b = 6.7555(1) \text{ \AA}$, $c = 12.5547(2) \text{ \AA}$, $V = 869.7190 \text{ \AA}^3$, respectively. The mean Y–O distances for $\text{Y}^{3+}(1)$ (CN = 6) and $\text{Y}^{3+}(2)$ (CN = 7) from the XRD refinement are estimated to be 2.2955 \AA and 2.4147 \AA , respectively. It was reported that there exist two different Y^{3+} sites with local symmetry C_1 : $\text{Y}^{3+}(1)$ site is six-coordinated with four silicon-bonded oxygen atoms and two non-silicon-bonded oxygen atoms (free oxygen atom); $\text{Y}^{3+}(2)$ site is seven-coordinated with five silicon-bonded oxygen atoms and two free oxygen atoms [19]. Since the ionic radius of Yb^{3+} (1.01 \AA at CN = 6 and 1.07 \AA at CN = 7) is very similar to those of Y^{3+} (1.04 \AA at CN = 6 and 1.1 \AA at CN = 7) [20], it is likely that the Yb^{3+} equally distributes over the two sites. In contrast,

Ce³⁺ (1.15 Å at CN = 6 and 1.21 Å at CN = 7) is significantly bigger and one can imagine that Ce³⁺ more easily enters the Y³⁺(2) site which is larger and more distorted than Y³⁺(1) site. From Table 1, one can see that the refined occupation fractions of Ce³⁺ are 0.0653 (Ce_{Y1}) and 0.2347 (Ce_{Y2}) out of 0.3, Yb³⁺ ions are 0.026 (Yb_{Y1}) and 0.034 (Yb_{Y2}) out of 0.06. These results indeed support the conclusions that more Ce³⁺ ions occupy the Y³⁺(2) site, and Yb³⁺ ions have no bias for these two non-equivalent C₁ symmetry Y³⁺ sites, which are consistent with previous results of electron paramagnetic resonance (EPR) and spectroscopic studies [21–23].

Table 1. Final Refined Structural Parameters for Y_{1.64}Ce_{0.3}Yb_{0.06}SiO₅^a

Atoms	Site	x	y	z	Occ.	B _{iso} (Å ²) ^b
Y1	8f	0.3070(2)	0.3757(2)	0.1422(1)	0.9087	1.25(4)
Ce1	8f	0.3070(2)	0.3757(2)	0.1422(1)	0.0653	1.25(4)
Yb1	8f	0.3070(2)	0.3757(2)	0.1422(1)	0.026	1.25(4)
Y2	8f	0.4270(2)	0.2522(2)	0.0381(1)	0.7313	1.20(4)
Ce2	8f	0.4270(2)	0.2522(2)	0.0381(1)	0.2347	1.20(4)
Yb2	8f	0.4270(2)	0.2522(2)	0.0381(1)	0.034	1.20(4)
Si1	8f	0.3713(5)	0.0870(8)	0.1834(5)	1	0.70(9)
O1	8f	0.3061(7)	-0.277(1)	0.1216(6)	1	1.46(8)
O2	8f	0.4412(9)	-0.001(1)	0.0977(7)	1	1.46(8)
O3	8f	0.4695(8)	-0.140(1)	0.2942(8)	1	1.46(8)
O4	8f	0.2627(8)	0.067(1)	0.2014(6)	1	1.46(8)
O5	8f	0.3794(7)	0.398(1)	0.0170(6)	1	1.46(8)

^a Space group: I12/a1 (No. 15), Z = 8, a = 10.5267(2) Å, b = 6.7555(1) Å, c = 12.5547 (2) Å, V = 869.7190 Å³, R_p = 2.47%, R_{wp} = 3.66%, R_b = 1.47%.

^b Constraints were placed on the atomic displacement factors for Y1 = Ce1 = Yb1, Y2 = Ce2 = Yb2 and O1 = O2 = O3 = O4 = O5.

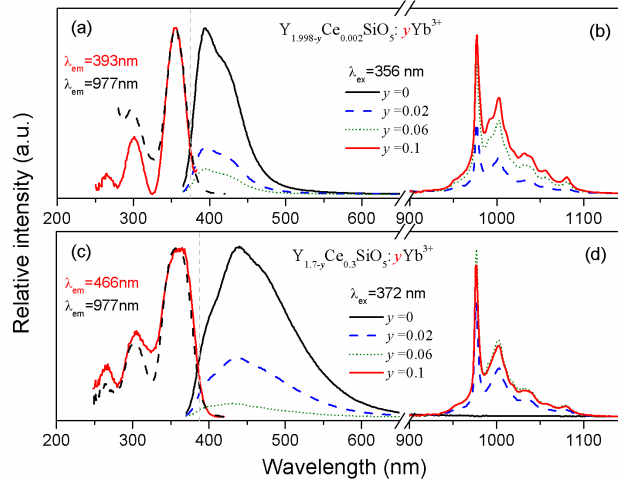


Fig. 3. (a), (c) Excitation, (b), (d) UV-vis and NIR emission spectra of Y_{1.998-y}Ce_{0.002}SiO₅:yYb³⁺ and Y_{1.7-y}Ce_{0.3}SiO₅:yYb³⁺. The visible and NIR emission intensities are not plotted on the same scale.

Photoluminescence properties of Y₂SiO₅:Ce³⁺ have been systematically discussed in the previous research [24–26]. It was found that Ce³⁺ ions enter two Y³⁺ sites and form two emission centers. Ce³⁺ at Y³⁺(2) site (CN = 7) has lower energy of 5d level than at Y³⁺(1) (CN = 6) due to the covalence effects [24], and here they are correspondingly labeled as “Ce³⁺(2)” and “Ce³⁺(1)”, respectively. Compared to Ce³⁺(1), the excitation and emission peaks of the Ce³⁺(2) should show a red-shift. In this work, we chose two Ce³⁺ concentrations (x = 0.002 and 0.3) for the research on the CET in Y_{2-x-y}SiO₅: xCe³⁺, yYb³⁺ phosphors. For x = 0.002, under the excitation of 356 nm from the lowest 5d level of Ce³⁺(1) center, the emission from Ce³⁺(1) is much stronger than that from Ce³⁺(2) (Fig. 3(b)); For x = 0.3, emission from Ce³⁺(2) is relatively stronger than that from Ce³⁺(1) when exciting the lowest 5d level at 372

nm of $\text{Ce}^{3+}(2)$ center (Fig. 3(d)). The maximum emission peak for $\text{Ce}^{3+}(1)$ is at 393 nm and $\text{Ce}^{3+}(2)$ at 466 nm, respectively, which well agrees with reported results [27,28]. Moreover, the position of the lowest 5d excited level of two Ce^{3+} centers is estimated by using the mirror-image relationship between the emission and the excitation spectra at 10 K [29]. The low temperature spectra were not given here due to their similarity with room temperature spectra (Fig. 3). From the intersection point of normalized excitation and emission spectra (10 K), the values of the lowest 5d energy level are evaluated to be at about 26740 cm^{-1} (374 nm) for $\text{Ce}^{3+}(1)$ ion and 25970 cm^{-1} (385 nm) for $\text{Ce}^{3+}(2)$ ion, which are close to twice the energy (20470 cm^{-1}) of ${}^2\text{F}_{7/2} \rightarrow {}^2\text{F}_{5/2}$ of Yb^{3+} . It is therefore expected that CET from Ce^{3+} to Yb^{3+} would occur in Y_2SiO_5 host. Hereafter, we will examine whether the CET process happens and to what extent 5d energy locations of Ce^{3+} ion play a role in the process.

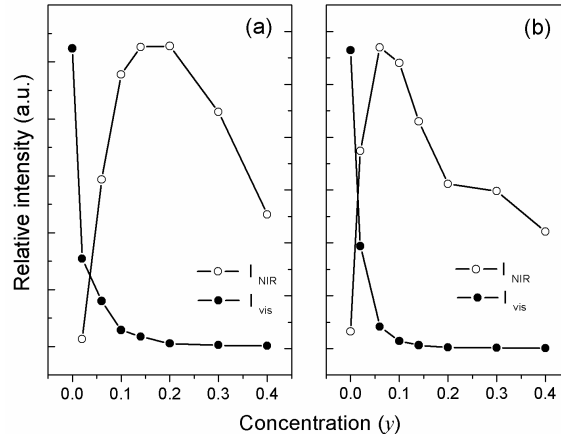


Fig. 4. Dependences of the integrated NIR and Vis emission intensity of (a) $\text{Y}_{1.998-y}\text{Ce}_{0.002}\text{SiO}_5:y\text{Yb}^{3+}$ ($\lambda_{\text{ex}} = 356 \text{ nm}$) and (b) $\text{Y}_{1.7-y}\text{Ce}_{0.3}\text{SiO}_5:y\text{Yb}^{3+}$ ($\lambda_{\text{ex}} = 372 \text{ nm}$) on the concentration (y) of Yb^{3+} . The integrated visible and NIR emission intensities are not plotted on the same scale.

When Yb^{3+} ions are present in the samples of the same Ce^{3+} content, regardless of $x = 0.002$ or 0.3 , it is obviously seen that the shape of PLE spectra changes little whenever the 977 nm emission of Yb^{3+} or the blue emission of Ce^{3+} is monitored. Beside the ${}^2\text{F}_{5/2} \rightarrow 5d$ absorption transition of Ce^{3+} , the charge transfer band (CTB, around 260 nm) of $\text{Yb}^{3+}\text{-O}^{2-}$ is not obviously observed in the PLE spectra. We performed excitation at 356 nm for $x = 0.002$ and 372 nm for $x = 0.3$ to avoid the interplay of the lowest 5d levels of both Ce^{3+} centers as much as possible. The PL results show that intense NIR emission of Yb^{3+} centering at 977 nm was observed, in addition to the violet-blue broadband emission of Ce^{3+} , as presented in Fig. 3(b) and 3(d). These evidences together persuaded us to believe that the energy transfer from Ce^{3+} to Yb^{3+} does take place. In order to confirm this speculation, the Yb^{3+} concentration dependence of visible and NIR emission intensity of the two series of samples were investigated in details and plotted in Fig. 4. As the concentration of Yb^{3+} ions increases, the integrated emission intensity of Ce^{3+} remarkably decreases and the NIR emission intensity of Yb^{3+} ions initially increases and then decreases due to concentration quenching. The optimum doping concentrations (y) for Yb^{3+} were accordingly determined to be 0.2 and 0.06 in $\text{Y}_{1.998-y}\text{Ce}_{0.002}\text{SiO}_5:y\text{Yb}^{3+}$ and $\text{Y}_{1.7-y}\text{Ce}_{0.3}\text{SiO}_5:y\text{Yb}^{3+}$, respectively. This further proves that the absorbed energy of Ce^{3+} can be partially transferred to a pair of nearest-neighbor Yb^{3+} ions, inducing NIR emission from ${}^2\text{F}_{5/2} \rightarrow {}^2\text{F}_{7/2}$ of Yb^{3+} through CET, as expected.

Like most $\text{Ce}^{3+}\text{-Yb}^{3+}$ systems, QC mechanism for $\text{Y}_2\text{SiO}_5:\text{Ce}^{3+}, \text{Yb}^{3+}$ can be generally described as Fig. 5. Under UV light excitation, electrons on the Ce^{3+} ions are excited from the ground state (4f) to the excited state (5d) (process ①). In the excited state, part of electrons relax to the lowest 5d excited state (process ②), then return to the ground state, generating the blue emissions (process ④). The other electrons in the excited 5d state of a Ce^{3+} ion cooperatively transfer their energy to two Yb^{3+} ions by downconversion (process ③).

Subsequently, electrons on the excited level ($^2F_{5/2}$) of Yb^{3+} ions return to the ground state ($^2F_{7/2}$), giving the NIR emissions (process ⑤). Competition between the above two processes (② \rightarrow ④ and ③ \rightarrow ⑤) results in the occurrence of emissions from Ce^{3+} and Yb^{3+} simultaneously in $\text{Y}_2\text{SiO}_5:\text{Ce}^{3+}$, Yb^{3+} samples (Fig. 4(b) and 4(d)). The entire direct CET process could be expressed as (① \rightarrow ③ \rightarrow ⑤).

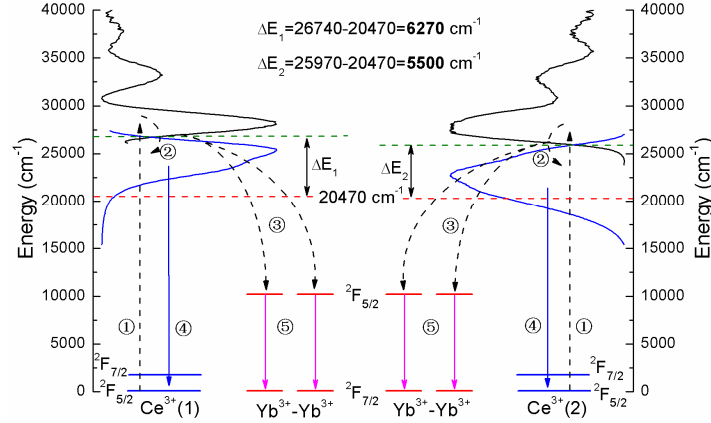


Fig. 5. Schematic energy level and cooperative energy transfer (CET) mechanism of Ce^{3+} and Yb^{3+} in Y_2SiO_5 host

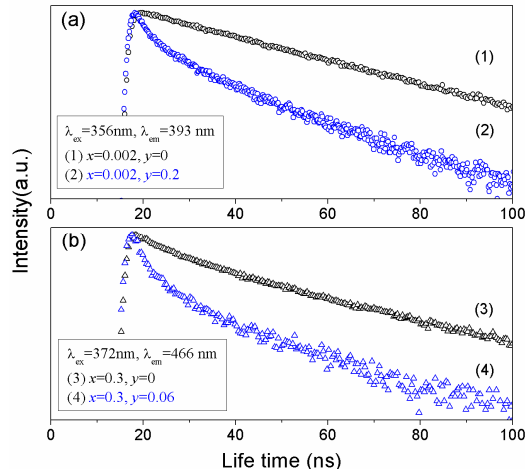


Fig. 6. Decay curves of (a) $\text{Y}_{1.998-y}\text{Ce}_{0.002}\text{SiO}_5: y\text{Yb}^{3+}$ phosphor ($y = 0$ and 0.2) and (b) $\text{Y}_{1.7-y}\text{Ce}_{0.3}\text{SiO}_5: y\text{Yb}^{3+}$ phosphor ($y = 0$ and 0.06)

As we pointed out in the introduction, the QC process in Ce^{3+} - Yb^{3+} couple should strongly depend on the $5d$ energy level of Ce^{3+} ion in some specific compounds. In the present case, the lowest $5d$ energy level is at about 26740 cm^{-1} for $\text{Ce}^{3+}(1)$ ion and 25970 cm^{-1} for $\text{Ce}^{3+}(2)$ ion. The energy differences (ΔE_1 and ΔE_2) between the lowest $5d$ energy level and twice the energy (20470 cm^{-1}) of $^2F_{5/2}$ level of Yb^{3+} are 6270 cm^{-1} for $\text{Ce}^{3+}(1)$ ion and 5500 cm^{-1} for $\text{Ce}^{3+}(2)$ ion. Comparatively, it is expected that multiple phonons-assisted CET process would be more efficient in $\text{Ce}^{3+}(2)$ - Yb^{3+} than in $\text{Ce}^{3+}(1)$ - Yb^{3+} couple, which is supported by the lifetime data, which we will discuss later.

For $\text{Y}_{1.998}\text{Ce}_{0.002}\text{SiO}_5$ and $\text{Y}_{1.7}\text{Ce}_{0.3}\text{SiO}_5$ phosphors, both $\text{Ce}^{3+}(1)$ or $\text{Ce}^{3+}(2)$ have a single-exponential decay behavior (Curves 1 and 3) as shown in Fig. 6. The lifetimes (τ) of $\text{Ce}^{3+}(1)$ and $\text{Ce}^{3+}(2)$ ions are estimated to be about 34.2 ns and 30.7 ns , respectively. The difference in

decay behavior may be due to local symmetry of the host lattice [30]. When Yb^{3+} ions are co-doped, the decay curves of $\text{Ce}^{3+}(1)$ and $\text{Ce}^{3+}(2)$ exhibit obvious nonexponential feature (Curves 2 and 4) and the lifetime of Ce^{3+} decrease gradually as Fig. 7(a) shows. This indicates there is an extra pathway for $5d$ electrons of either $\text{Ce}^{3+}(1)$ or $\text{Ce}^{3+}(2)$ to depopulate. The rate equation for the population densities of the excited $5d$ state of Ce^{3+} can be expressed as follows [31]

$$\frac{dN_{Ce}}{dt} = \frac{N_{Ce}}{\tau_0} - K_{Ce \rightarrow Yb} N_{Ce} = -\left(\frac{1}{\tau_0} + K_{Ce \rightarrow Yb}\right) N_{Ce} = -\frac{N_{Ce}}{\tau} \quad (1)$$

$$K_{Ce \rightarrow Yb} = \frac{1}{\tau} - \frac{1}{\tau_0} \quad (2)$$

where N_{Ce} is the population densities in the excited $5d$ state within the Ce^{3+} ion, τ_0 the intrinsic fluorescence lifetime of Ce^{3+} ($y = 0$), $K_{Ce \rightarrow Yb}$ the nonradiative energy-transfer rate from the $5d$ state of Ce^{3+} to the ${}^2F_{5/2}$ energy level of Yb^{3+} , and τ the Ce^{3+} donor lifetimes in the presence of Yb^{3+} acceptor. Furthermore, the CET efficiency (η_{CET}) and the total theoretical down-conversion quantum efficiency (η_{QE}) can be defined as below [10, 12]

$$\eta_{CET} = 1 - \frac{\tau}{\tau_0} \quad (3)$$

$$\eta_{QE} = \eta_{Ce} (1 - \eta_{CET}) + 2\eta_{Yb} \eta_{CET} \quad (4)$$

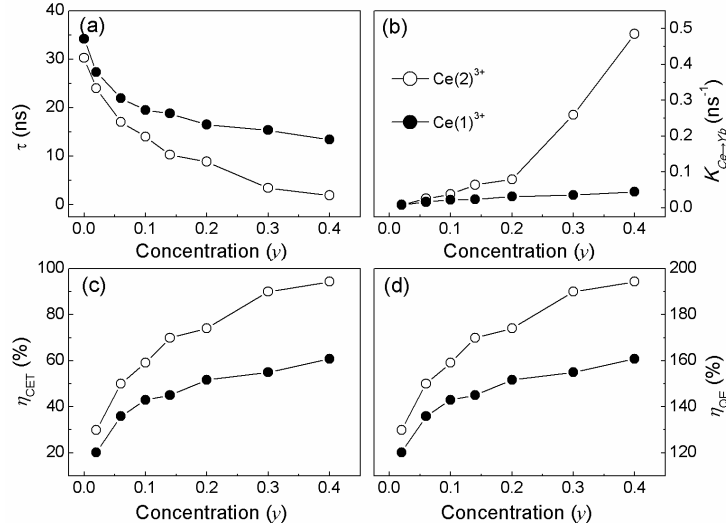


Fig. 7. (a) Decay lifetime (τ) of Ce^{3+} , (b) nonradiative energy-transfer rate ($K_{Ce \rightarrow Yb}$), (c) CET efficiency (η_{CET}) and (d) quantum efficiency (η_{QE}) as a function of Yb^{3+} concentration (y) in $\text{Y}_{1.998-y}\text{Ce}_{0.002}\text{SiO}_5: y\text{Yb}^{3+} [\text{Ce}^{3+}(1)]$ and $\text{Y}_{1.7-y}\text{Ce}_{0.3}\text{SiO}_5: y\text{Yb}^{3+} [\text{Ce}^{3+}(2)]$, respectively.

Figures 7(b), 7(c) and 7(d) demonstrate the dependences of $K_{Ce \rightarrow Yb}$, η_{CET} and η_{QE} on the concentration of Yb^{3+} ions, respectively. It can be clearly observed that, the CET rate and efficiencies of $\text{Ce}^{3+}(1) \rightarrow \text{Yb}^{3+}$ and $\text{Ce}^{3+}(2) \rightarrow \text{Yb}^{3+}$ and the quantum efficiency (η_{QE}) increase as the concentration of Yb^{3+} ions increases. The difference between $\text{Ce}^{3+}(1) \rightarrow \text{Yb}^{3+}$ and $\text{Ce}^{3+}(2) \rightarrow \text{Yb}^{3+}$ is that the increasing trends of the CET rate and efficiencies are more obvious in $\text{Ce}^{3+}(2) \rightarrow \text{Yb}^{3+}$ than in $\text{Ce}^{3+}(1) \rightarrow \text{Yb}^{3+}$, suggesting that the CET process between $\text{Ce}^{3+}(2)$ and Yb^{3+} is more efficient. Additionally, the quantum efficiency η_{QE} could be estimated by Eq. (4), where η_{Ce} and η_{Yb} stand for the quantum efficiency of Ce^{3+} and Yb^{3+} , respectively.

Assuming that all the excited Yb^{3+} ions and the residual excited Ce^{3+} ions decay radiatively, i.e., $\eta_{\text{Ce}} = \eta_{\text{Yb}} = 1$ [10], the upper limited values of the highest total DC quantum efficiency (η_{QE}) are calculated to be 161% for $\text{Ce}^{3+}(1)\text{-Yb}^{3+}$ couple and 194% for $\text{Ce}^{3+}(2)\text{-Yb}^{3+}$, respectively.

Since other key factors, such as phonon vibration frequency, crystal structure and Yb^{3+} ion occupation fractions, are kept constant in the same $\text{Y}_{2-x}\text{Ce}_x\text{Yb}_y\text{SiO}_5$ material, the CET efficiency and QE mainly depend on the energy locations of $5d$ orbital of Ce^{3+} in $\text{Ce}^{3+}\text{-Yb}^{3+}$ system. The as-obtained results show that the smaller ΔE between the lowest $5d$ orbital of Ce^{3+} and twice the ${}^2\text{F}_{5/2}\text{-}{}^2\text{F}_{7/2}$ transition energy ($\sim 20000\text{ cm}^{-1}$) of Yb^{3+} results in higher CET efficiency and QE. As well known, $\text{Ce}^{3+}\text{-Yb}^{3+}$ is an efficient donor-acceptor pair with high potential as a full spectrum converter for Si solar cells. Therefore, we believe that our effort may open a new route to the design of advanced UV/Vis-to-NIR phosphors for Si based solar cell applications.

3. Conclusions

We have systematically studied the effects of the location of the lowest $5d$ energy level of Ce^{3+} centers on the NIR QC process in $\text{Y}_2\text{SiO}_5\text{:Ce}^{3+}, \text{Yb}^{3+}$. The $\text{Ce}^{3+}(1)$ and $\text{Ce}^{3+}(2)$ centers dominate the emission spectra at low and high Ce^{3+} -concentration in Y_2SiO_5 , respectively. Phonon-assisted QC processes occur within both $\text{Ce}^{3+}(1)\text{-Yb}^{3+}$ and $\text{Ce}^{3+}(2)\text{-Yb}^{3+}$ couples, which contribute to the utilization of the UV-green fraction ($300 < \lambda < 500\text{ nm}$) of the solar spectrum and the consequent enhancement of the NIR emission intensity of Yb^{3+} ions. As the concentration of Yb^{3+} increases, the lifetimes of $\text{Ce}^{3+}(1)$ and $\text{Ce}^{3+}(2)$ decrease, and nonradiative energy transfer rate ($K_{\text{Ce}\rightarrow\text{Yb}}$), CET efficiency (η_{CET}) and quantum efficiency (η_{QE}) increase. Additionally, the estimated highest total η_{QE} is 161% for $\text{Ce}^{3+}(1)\text{-Yb}^{3+}$ couple and 194% for $\text{Ce}^{3+}(2)\text{-Yb}^{3+}$, respectively. Most importantly, it was found that if the energy location of the lowest $5d$ excited state of Ce^{3+} center is closer to twice the ${}^2\text{F}_{7/2}\text{-}{}^2\text{F}_{5/2}$ absorption energy ($\sim 20000\text{ cm}^{-1}$) of Yb^{3+} , the CET efficiency is higher. Therefore, from the point of enhancing the efficiency of silicon-based solar cells, we suggest to exploit new solar spectra-converters involving $\text{S}^{n+}\text{-Yb}^{3+}$ couple, where S^{n+} is a cation sensitizer that can efficiently absorb solar lights in the UV and visible region and has its dominating depopulation level located at around 20000 cm^{-1} .

Acknowledgments

This work was supported by the National High Technology Research and Development Program of China (2010AA03A404), National Natural Science Foundation of China (20971130, 20871121, 10979027), the Fundamental Research Funds for the Central Universities (091GPY19, 111GJC07), the Open Fund of the State Key Laboratory of Optoelectronic Materials and Technologies (Sun Yat-sen University, 2010-ZY-03), Guangdong Provincial Science & Technology Project (2010A011300004) and the Science and Technology Project of Guangzhou (11A34041302).